Supporting Information

Deciphering the structure of tungstate and molybdate complexes with glucose, mannose and erythrose

Sabah El Mohammad[a], Sandrine Develle,[a] Olivier Proux[b], Antonio Aguilar[c], Jean-Louis Hazemann[d], Christèle Legens[a], Céline Chizallet[a], Kim Larmier[a,*]

Corresponding author : Kim Larmier (email kim.larmier@ifpen.fr)

[a] *IFP Energies nouvelles, Rond-Point de l'Echangeur de Solaize, 69360 Solaize, France.*
[b] *OSUG, UAR 832 CNRS, Université Grenoble Alpes, 38041, Grenoble, France.*
[c] *ICMG, UAR 2607 CNRS, Université Grenoble Alpes, 38041, Grenoble, France.*
[d] *Institut Néel, CNRS, Université Grenoble Alpes, 25 Avenue des Martyrs, 38042 Grenoble, France.*

Experimental details

NMR spectroscopy

All NMR spectra were recorded on a Bruker Avance III spectrometer (300 MHz) equipped with a Broadband probe (BBFO) at 300 K and processed using Bruker TopSpin 3.6.3.

1D-NMR Spectra: The applied frequencies were respectively 300.13 and 75.47 MHz for ^{1}H and ^{13}C nuclei. ^{1}H NMR chemical shifts were referenced using residual solvent peak for proton resonance of deuterium oxide (4.79 ppm). Proton spectra were obtained with an acquisition time of 3.4 s, a pulse duration of 14 µs with 6.7 W power pulse force and a sweeping range of 4807.7Hz. The relaxation delay was of 2 s. 1D proton decoupled ^{13}C spectra were recorded with the following parameters: acquisition time of 1.66 s, pulse duration of 9 µs with 38.8 W power pulse force, relaxation delay of 2 s and a sweeping range of 19736.8 Hz. In both experiments, the number of scans was adjusted according to the sample. ^{95}Mo NMR spectra were recorded at 19.95 MHz at 300K. The ^{95}Mo experiments used aring pulse sequence (in the Bruker TopSpin 3.6.3 pulse program library), with 25 ms relaxation delay (d1), 29 ms acquisition time (aq), and a sweep-width (sw) of 34.7 kHz. Chemical shifts (δ) are reported in ppm relative to Na_2MoO_4 (0.1 M) in D_2O. When only sharp peaks were observed, an additional spectrum was recorded with d1 = 2 s and acquisition time of 1.88 s.

2-D NMR spectra: The 2D ^{1}H-^{1}H correlation spectroscopy (COSY) spectra were acquired using the following acquisition parameters: 1 scan, 16 dummy scans, a 1.3 s relaxation delay, a spectral width of 3.7 ppm, a transmitter offset of 5 ppm, and an acquired spectral size of 512 data points in the F1 dimension and of 2048 data points in the F2 dimension. The 2D ^{1}H-^{13}C heteronuclear single quantum correlation (HSQC) spectra were obtained with the following acquisition parameters: 2 scans, 16 dummy scans, a 1.5 s relaxation delay, a spectral width of 3.7 ppm (F2) and 180 ppm (F1), a transmitter offset of 5 ppm (F2) and 90 ppm (F1), a mean coupling constant $^{1}J_{C-H}$ for the intensive nuclei enhanced by polarization transfer (INEPT) to 145 Hz, an acquired spectral size of 256 data points in the F1 dimension and 1024 data points in the F2 dimension.

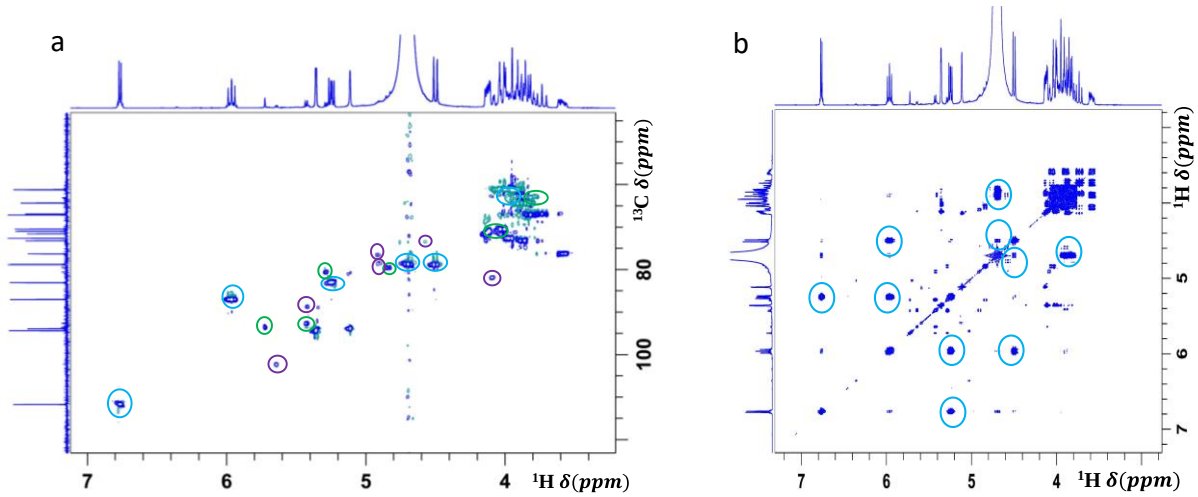

Figure S1. *(a) heteronuclear single quantum correlation ^{1}H-^{13}C NMR spectrum, (b) ^{1}H homonuclear NMR correlation spectrum of a solution of sodium tungstate with D-mannose at pH 7.1, mannose and tungsten concentrations of 1 and 2 mol.L^{-1} respectively. The circles depicted in the 2D spectra correspond to the correlation between the carbon atoms and the proton(s) attached to them in addition to the correlation between vicinal protons respectively in the HSQC and the COSY spectra. Cyan : Complex A, Green : Complex B, Purple: Complex C. Reproduced from ref [1]*

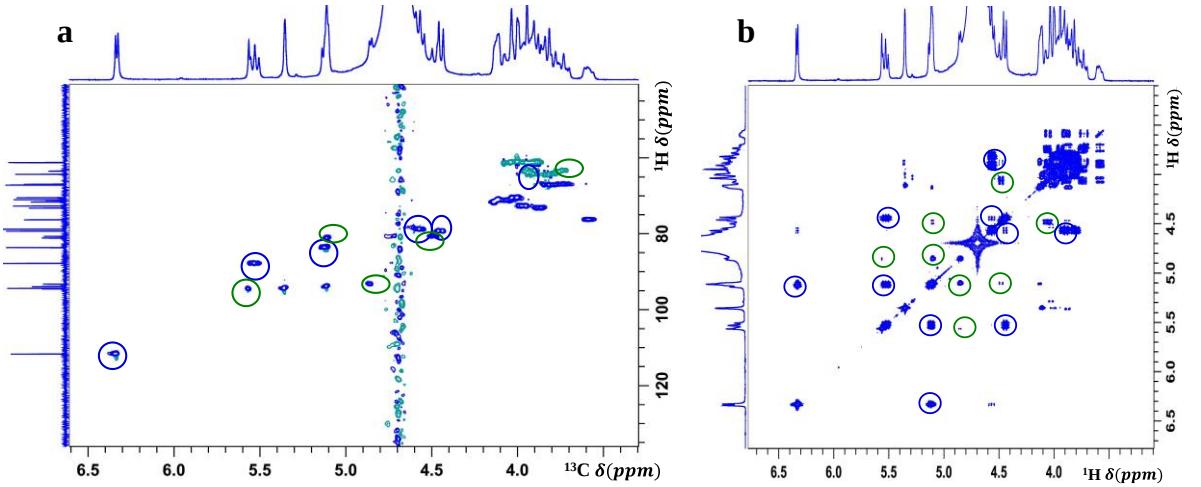

Figure S2. *(a) heteronuclear single quantum correlation ^{1}H-^{13}C NMR spectrum, (b) ^{1}H homonuclear NMR correlation spectrum of a solution of sodium molybdate with D-mannose at pH 6.4, mannose and molybdenum concentrations of 1 and 2 mol.L^{-1} respectively. The circles depicted in the 2D spectra correspond to the correlation between the carbon atoms and the proton(s) attached to them in addition to the correlation between vicinal protons respectively in the HSQC and the COSY spectra.*

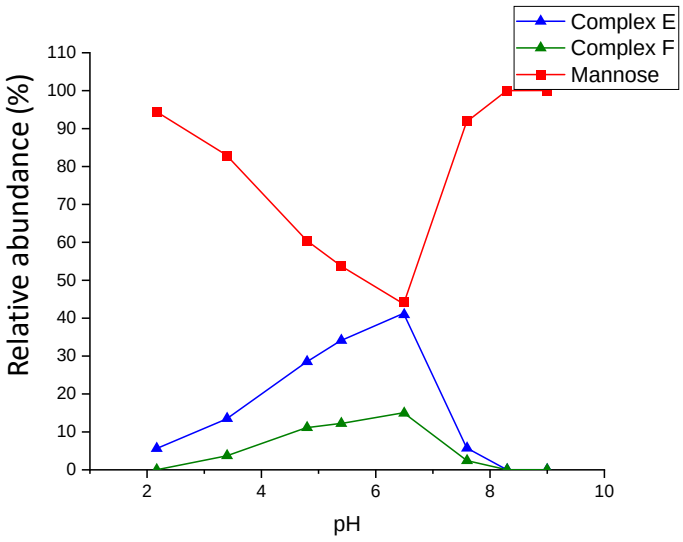

Figure S3. *Concentration of Complexes E and F in a series of sodium molybdate and mannose solutions as function* of *pH (molybdenum and mannose concentrations of 2 and 1 mol.L^{-1} respectively).*

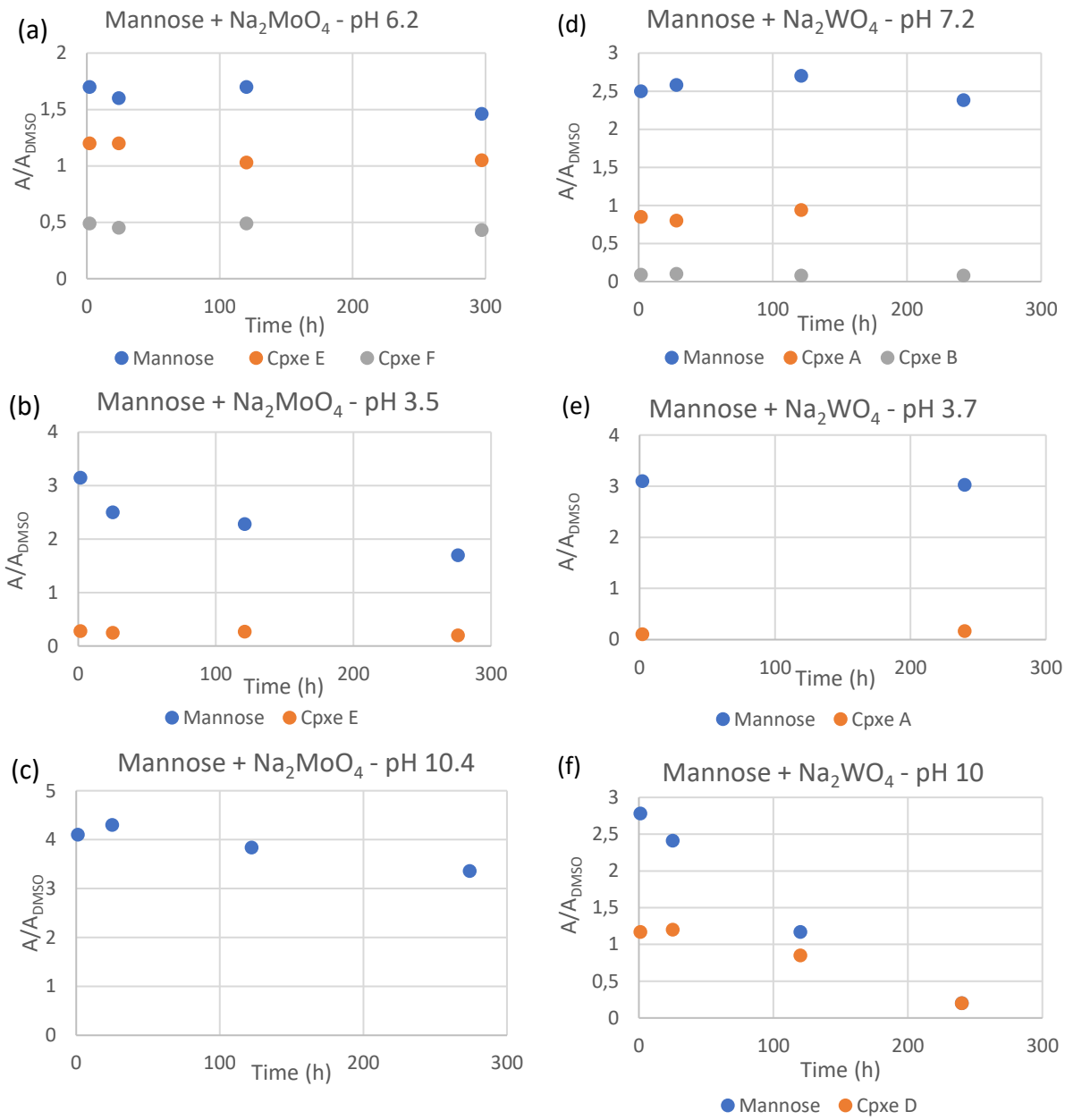

Figure S4. *Evolution over time at room temperature of the peak area in ^{13}C NMR of the various species w.r.t. that of DMSO (39.5 ppm) in various cases. (a,b,c) Mannose-Na_2MoO_4 mixtures at different pH. (d,e,f) Mannose-Na_2WO_4 mixtures at different pH. In all cases, [M] = 2 mol L^{-1}, [sugar] = 1* mol L^{-1}.

In the series of experiment presented on Figure S4, the mixtures were prepared according to the preparation method detailed above, and then introduced in NMR tubes equipped with an insert containing a 0.5 M solution of DMSO in D_2O. The same amount of solution is introduced in each tube, so that the peak of DMSO serves as an internal standard. Though the exact quantity of DMSO in each tube may vary slightly, it remains stable over time and is approximately similar in all tubes, so that this method affords a qualitative assessment of the stability of the species and to verify that they are not minor species only. Note that we additionally carried out determination of the absolute concentrations of species at the beginning of the experiments by dissolving the sugar and metallic species in the DMSO solution and measured the NMR spectra after 30 minutes in independent experiments. The sum of concentrations of species detected amount to about 1.0 ± 0.1 mol L^{-1} in all cases for glucose and mannose.

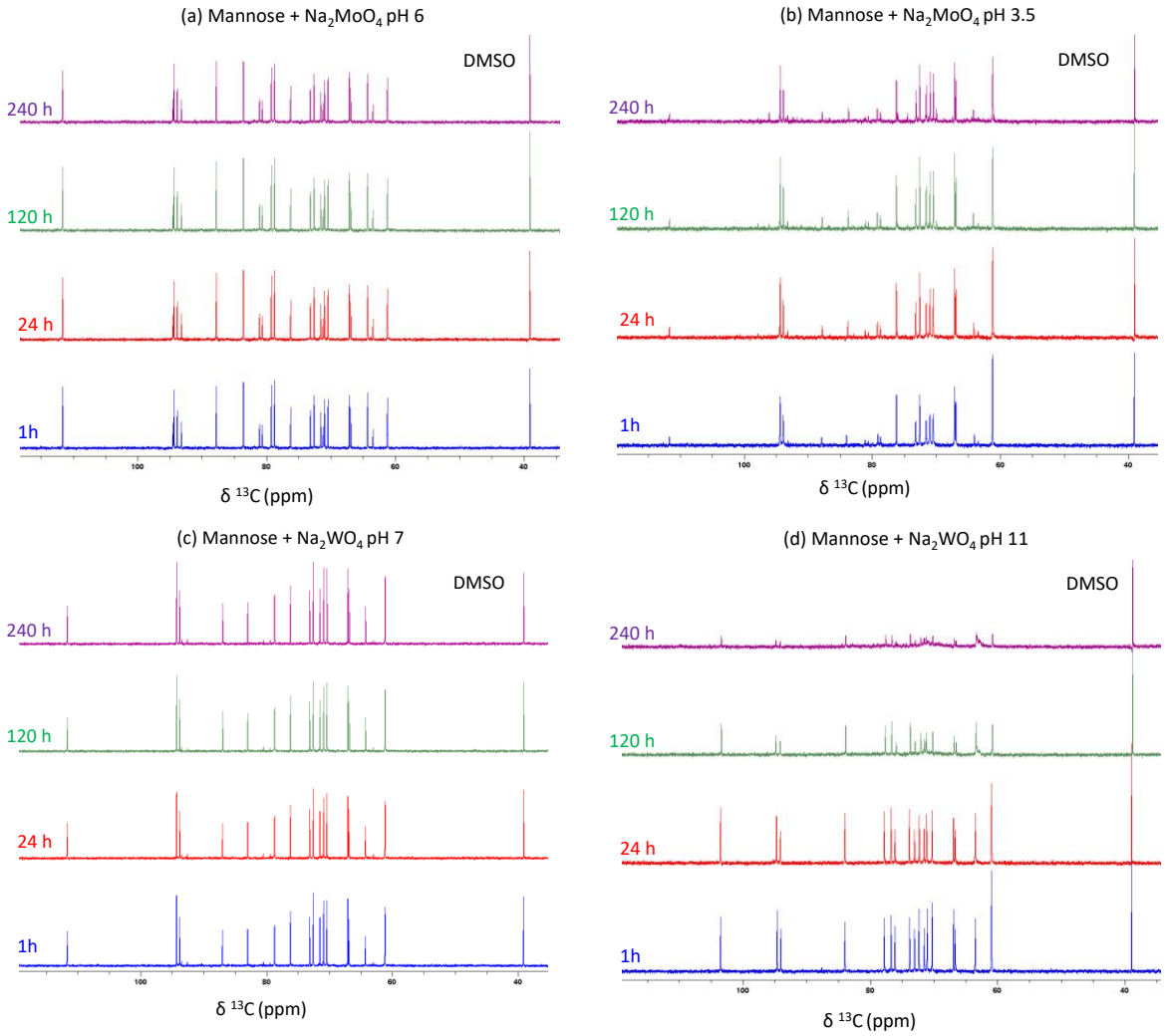

Figure S5. Selection of ^{13}C NMR spectra corresponding to the data on **Figure S10**, scaled on the signal of the standard DMSO. Mixtures of mannose and (a,b) Na_2MoO_4 at (a) pH 6.0 (b) pH 3.5, and (c,d) Na_2WO_4 at (c) pH 7.0 and (d) pH 11.0.

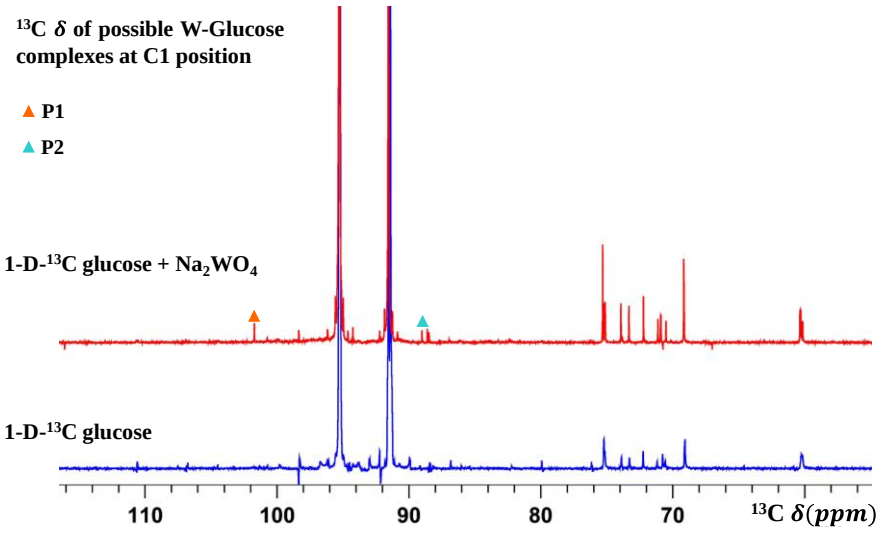

Figure S6. *Carbon decoupled NMR spectra of 1-^{13}C glucose aqueous solution with and without sodium tungstate (Na_2WO_4) at pH around 7.*

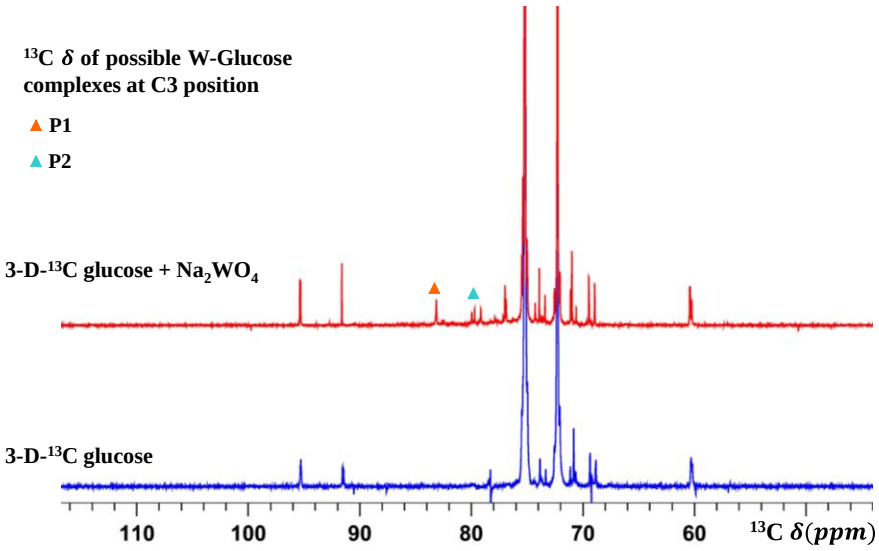

Figure S7. *Carbon decoupled NMR spectra of 3-^{13}C glucose aqueous solution with and without sodium tungstate (Na_2WO_4) at pH around 7.*

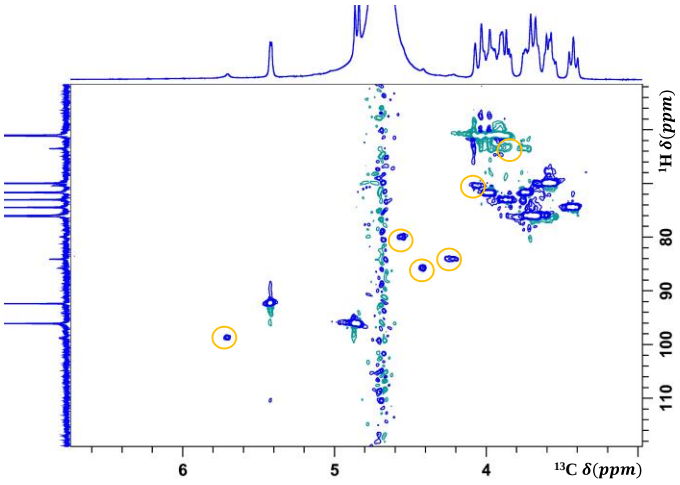

Figure S8. *Heteronuclear single quantum correlation ^{1}H-^{13}C NMR spectrum of a solution of sodium molybdate with D-glucose at pH 6.1, glucose and molybdenum concentrations of 1 and 2 mol.L^{-1} respectively. The orange circles depicted in the 2D spectra correspond to the correlations in Complex G between the carbon atoms and the proton(s) attached to them the HSQC spectrum.*

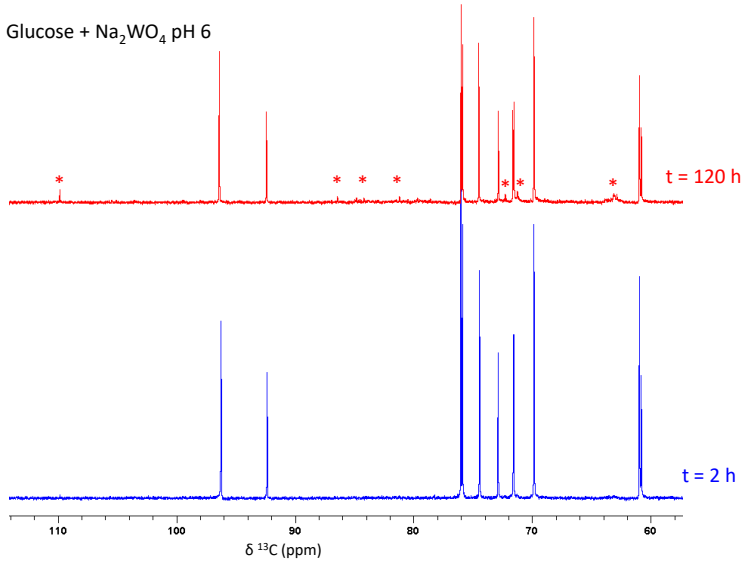

Figure S9.*Evolution of the ^{13}C NMR spectrum of glucose and Na_2WO_4 over 5 days.*

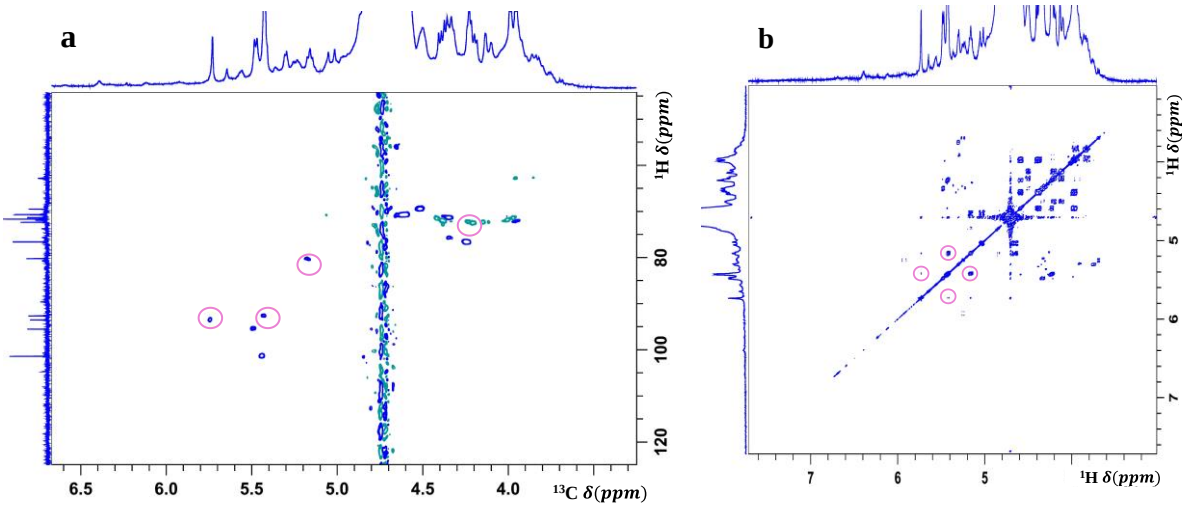

Figure S10. *(a) heteronuclear single quantum correlation ^{1}H-^{13}C NMR spectrum, (b) ^{1}H homonuclear NMR correlation spectrum of a solution of sodium tungstate with D-erythrose at pH around 7.2, erythrose and tungsten concentrations of 1 and 2 mol.L^{-1} respectively. The circles depicted in the 2D spectra correspond to the correlation between the carbon atoms and the proton(s) on Complex H.*

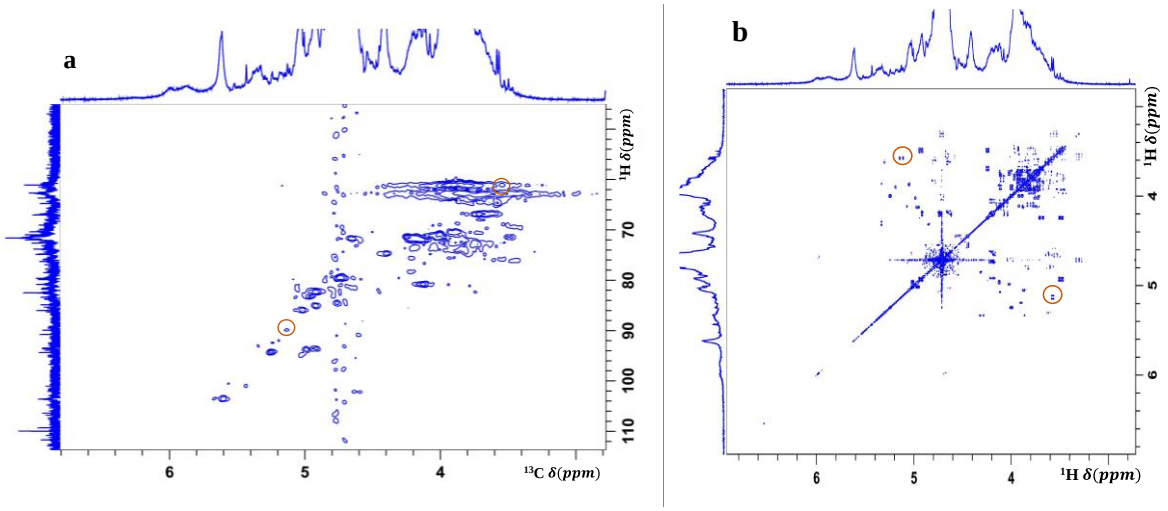

Figure S11. *(a) heteronuclear single quantum correlation ^{1}H-^{13}C NMR spectrum, (b) ^{1}H homonuclear NMR correlation spectrum of a solution of sodium tungstate with D-erythrose at pH = 10.3, erythrose and tungsten concentrations of 1 and 2 mol.L^{-1} respectively. The circles depicted in the 2D spectra correspond to the correlation possibly assigned to glycolaldehyde*

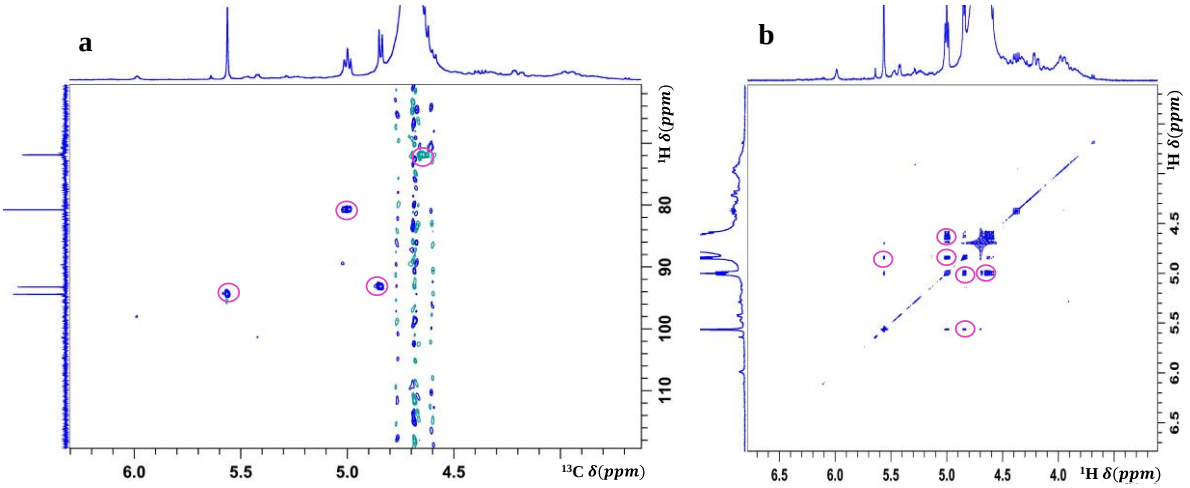

Figure S12. *(a) heteronuclear single quantum correlation ^{1}H-^{13}C NMR spectrum, (b) ^{1}H homonuclear NMR correlation spectrum of a solution of sodium molybdate with D-erythrose at pH 6.0, erythrose and molybdenum concentrations of 1 and 2 mol.L^{-1} respectively. The circles depicted in the 2D spectra correspond to the correlation between the carbon atoms and the proton(s) assigned to Complex I.*

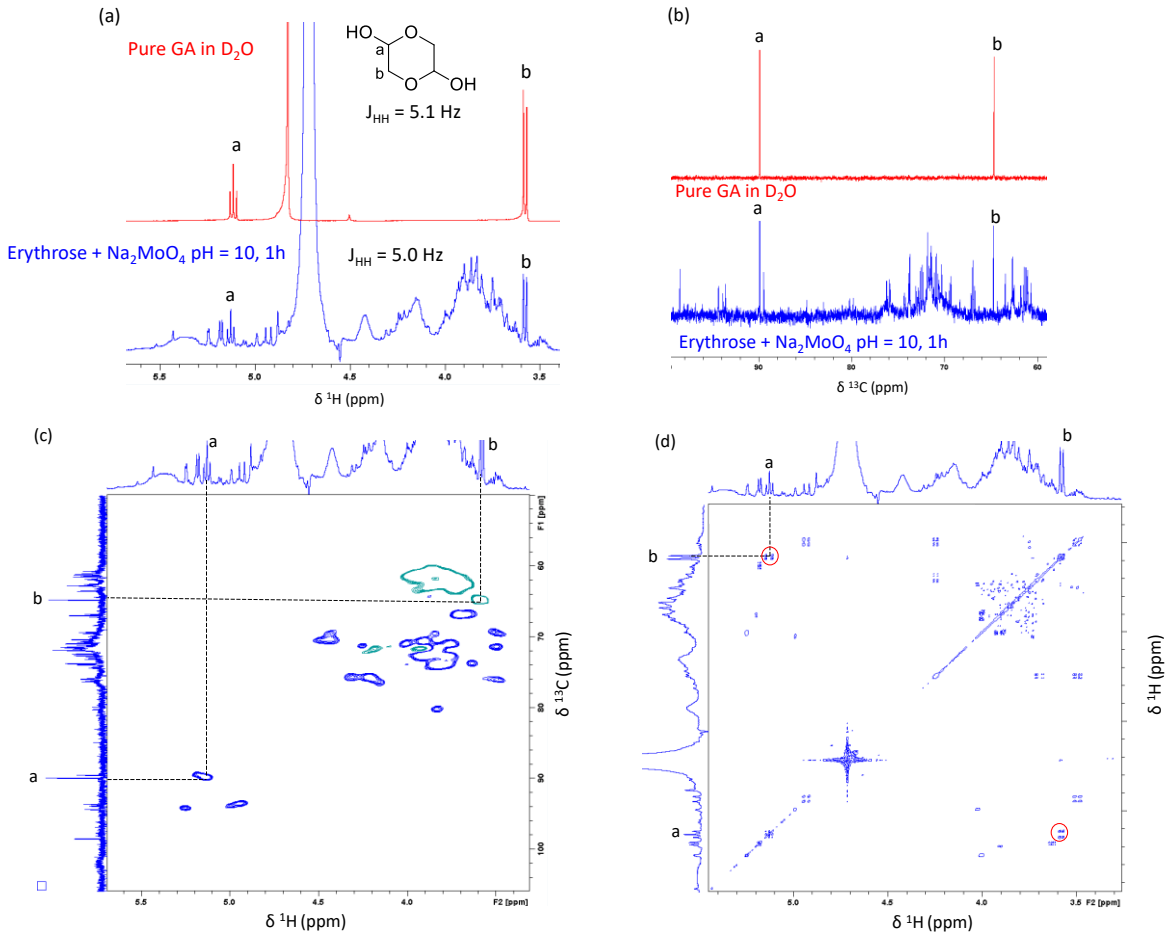

Figure S13. *NMR spectra taken for the combination of Erythrose and Na_2MoO_4 at pH = 10 one hour after the preparation of the sample (a) ^1H spectrum compared to that of pure glycolaldehyde in D_2O (b) ^{13}C spectrum (c) heteronuclear single quantum correlation ^1H-^{13}C NMR spectrum, (d) ^1H homonuclear NMR correlation spectrum of a solution of sodium molybdate with D-erythrose at pH = 10.4, erythrose and molybdenum concentrations of 1 and 2 mol.L^{-1} respectively. The circles depicted in the 2D spectra correspond to glycolaldehyde.*

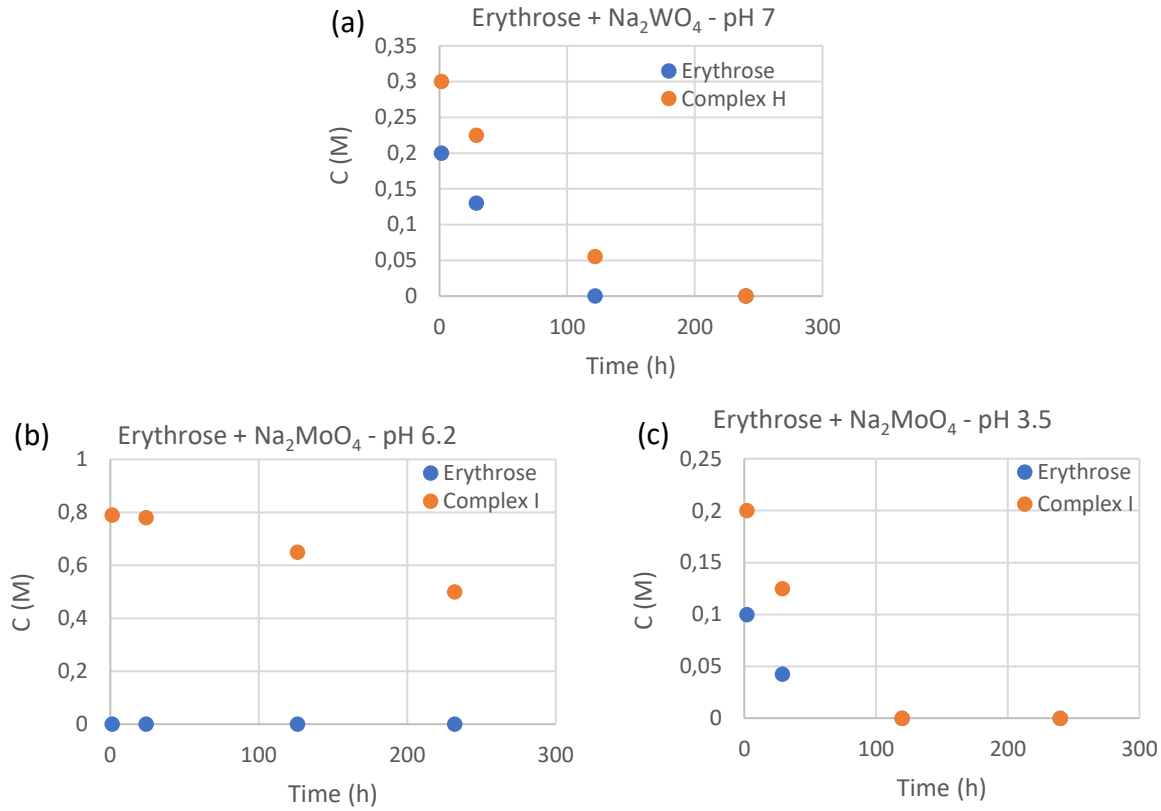

Figure S14. *Evolution over time at room temperature of the peak area in ^{13}C NMR of the various species in various cases with erythrose. In all cases, [M] = 2 mol L^{-1}, [sugar] = 0.5* mol L^{-1}. Aqueous mixtures of erythrose and (a) Na_2WO_4 at pH 7.0 (b) Na_2MoO_4 at pH 6.2 (c) $Na_{2Mo}O_4$ at pH 3.5.

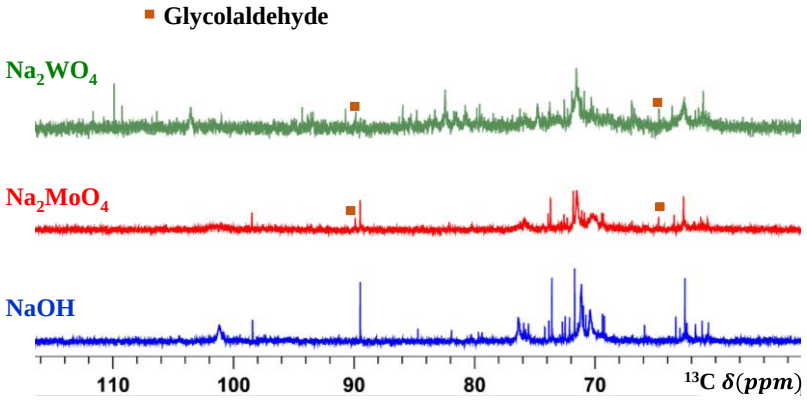

Figure S15. *Proton decoupled ^{13}C NMR spectrum of erythrose aqueous solution with different catalysts at pH= 10.5.*

Figure S16. *Aqueous molybdate speciation at total molybdate concentrations of 0.1 mol L^{-1} calculated using Medusa software and Hydra data base for the search of the possible inorganic complexes.*[2]

Figure S17. *Aqueous tungstate speciation at total tungstate concentrations of 0.1 mol L^{-1} calculated using Medusa software and Hydra data base for the search of the possible inorganic complexes.*[2]

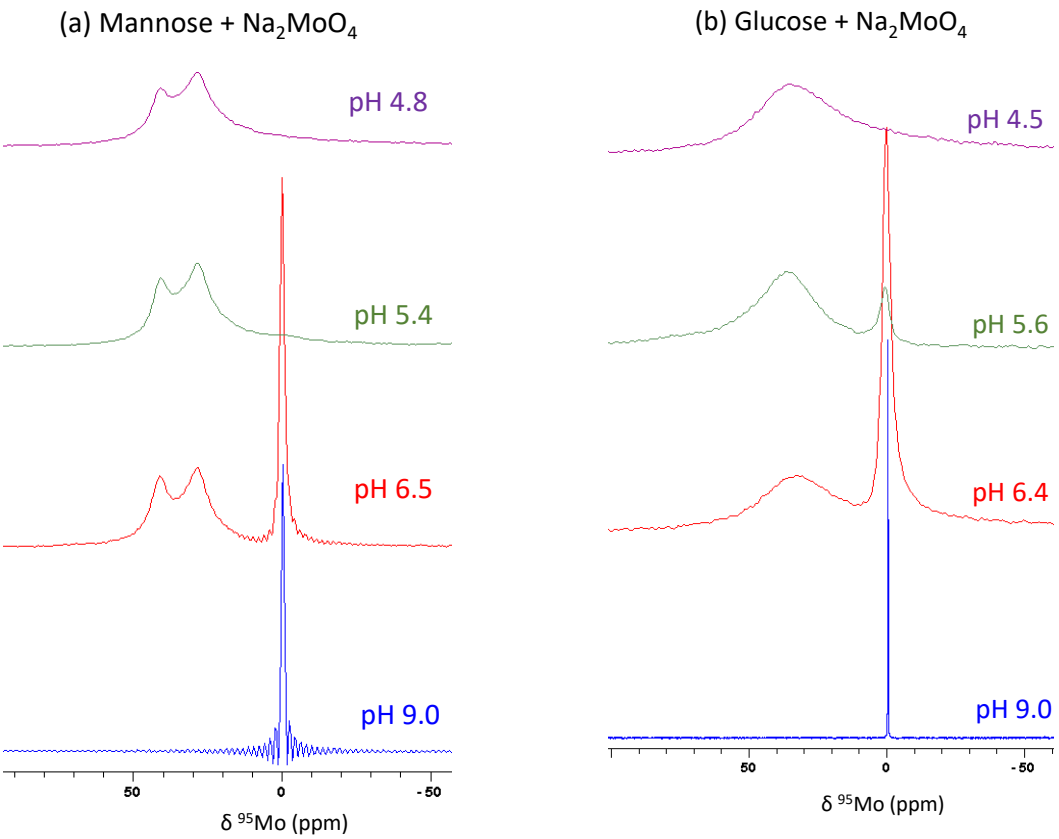

***Figure S18**. Evolution of the ^{95}Mo spectra of Na_2MoO_4 solutions with pH (a) mannose and (b) glucose ([M] = 2 mol L^{-1}, [sugar] = 1 mol L^{-1}). Oscillations on the spectrum for Mannose + Na_2MoO_4 at pH 9 are due to a too short acquisition time causing a truncation of the FID. This parameter was adapted in the other spectra.*

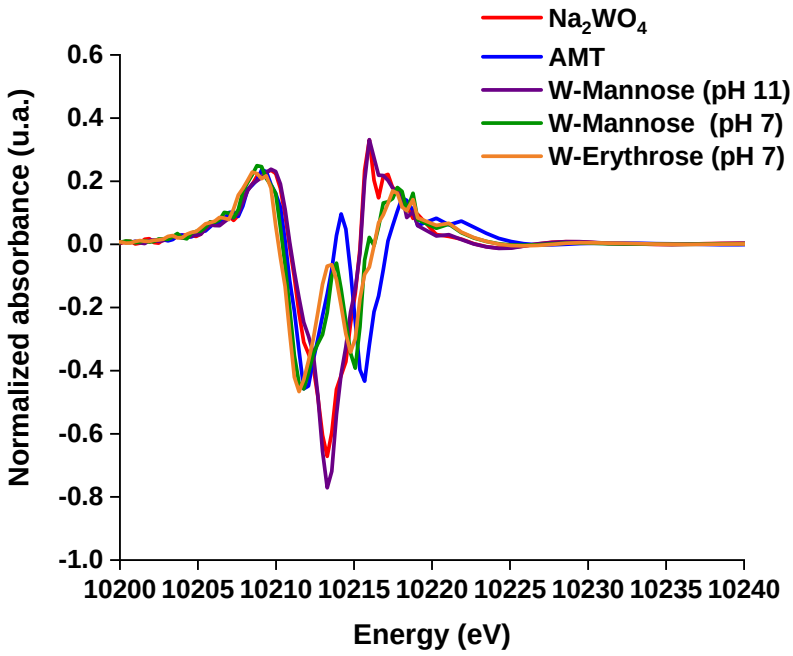

***Figure S19.** Second derivative of W-L_3 edge spectra of tungstate precursors and tungstate-sugars mixtures. Metal-sugars solutions were prepared at 2/1 metal/sugar ratio. [W] = 0.2 mol.L^{-1} and [sugar] = 0.1 mol.L^{-1}.*

Table S1. *^{13}C NMR chemical shifts (in ppm) of metal-sugars complexes. * Values taken from labeled glucose experiments with sodium tungstate at pH around 7 (**Figures S2** and **S3**). Previous results from the literature are also reported when available.*

Carbon atom	***C1***	***C2***	***C3***	***C4***	***C5***	***C6***
Tungstate-Mannose Complexes						
L Type[3]	112.7	84.0	88.0	79.7	79.7	65.2
M Type[3]	103.6	89.7	79.5	77.5	82.6	74.3
Complex A	111.7	83.2	87.1	78.8	78.7	64.3
Complex B	93.6	92.6	80.5	79.5	71.0	63.1
Complex C	102.6	88.6	78.5	76.6	81.9	73.4
Complex D	103.5	83.7	76.7	78.1	73.5	63.6
Molybdate-Mannose Complexes						
L Type[3]	112.2	84.1	88.3	79.7	79.3	64.8
A Type[3]	94.6	93.6	81.6	80.5	71.5	64.1
Complex E	111.6	83.5	87.7	79.2	78.7	64.3
Complex F	94.5	93.4	81.0	80.5	71.1	63.4
Tungstate-Glucose Complexes						
Complex P1	101.8*	nd	83.1*	nd	nd	nd
Complex P2	88.6*	nd	79.7*	nd	nd	nd
Molybdate-Glucose Complexes						
A Type[4,5]	99.7	86.8	80.8	85.1	71.2	64.4
Complex G	98.7	85.7	79.9	84.1	70.3	63.1
Tungstate-Erythrose Complexes						
Complex H	93.5	92.6	80.2	71.3	-	-
Molybdate-Erythrose Complexes						
A Type[6]	95.3	94.1	81.6	72.5	-	-
Complex I	94.3	93.2	80.6	71.8	-	-

Table S2. *Experimental ^{13}C NMR Chemical shifts (in ppm) of **complex E** and the corresponding experimental CIS value patterns of the assumed ligands. * Asterisk indicates a possible chelation site through an oxygen atom.*

Carbon atom	***C1***	***C2***	***C3***	***C4***	***C5***	***C6***
^{13}Cδ (Complex E)	**111.6**	**83.5**	**87.5**	**79.2**	**78.7**	**64.3**
^{13}Cδ α-pyranose[7]	95.4	72.0	71.5	68.1	73.7	62.3
CIS value	**16.2**	**11.5**	**16.0**	**11.1**	**5.0**	**2.0**
^{13}Cδ β-pyranose[7]	95.0	72.6	74.3	68.0	77.4	62.4
CIS value	**16.6**	**10.9**	**13.2**	**11.2**	**1.3**	**1.9**
^{13}Cδ α-furanose[3]	102.7	77.9	72.5	80.5	70.6	64.5
CIS value	**8.9**	**5.6**	**15.0**	**-1.3**	**8.1**	**-0.2**
^{13}Cδ β-furanose[3]	96.6	73.1	71.2	80.7	71.0	64.4
CIS value	**15.0***	**10.4***	**16.3***	**-1.5**	**7.7***	**-0.1**
^{13}Cδ Hydrate form[4,8]	90.6	74.2	71.6	71.6	74.2	65.8
CIS value	**21.0***	**9.3***	**15.9***	**7.6***	**4.5**	**-1.5**

Table S3. *Experimental ^{13}C NMR Chemical shifts (in ppm) of **complex F** and the corresponding experimental CIS value patterns of the assumed ligands. * Asterisk indicates a possible chelation site through an oxygen atom.*

Carbon atom	***C1***	***C2***	***C3***	***C4***	***C5***	***C6***
^{13}Cδ (Complex F)	**94.5**	**93.4**	**81.0**	**80.5**	**71.1**	**63.4**
^{13}Cδ α-pyranose[7]	95.4	72.0	71.5	68.1	73.7	62.3
CIS value	**-0.9**	**21.4**	**9.5**	**12.4**	**-2.6**	**1.1**
^{13}Cδ β-pyranose[7]	95.0	72.6	74.3	68.0	77.4	62.4
CIS value	**-0.5**	**20.8**	**6.7**	**12.5**	**-6.3**	**1.0**
^{13}Cδ α-furanose[3]	102.7	77.9	72.5	80.5	70.6	64.5
CIS value	**-8.2**	**15.5***	**8.5***	**0.0**	**0.5**	**-1.1**
^{13}Cδ β-furanose[3]	96.6	73.1	71.2	80.7	71.0	64.4
CIS value	**-2.1**	**20.3***	**9.8***	**-0.2**	**0.1**	**-1.0**
^{13}Cδ Hydrate form[4,8]	90.6	74.2	71.6	71.6	74.2	65.8
CIS value	**3.9***	**19.2***	**9.4***	**8.9***	**-3.1**	**-2.4**

Table S4. *Experimental ^{13}C NMR Chemical shifts (in ppm) of* ***complex G*** *and the corresponding experimental CIS value patterns of the assumed ligands. * Asterisk indicates a possible chelation site through an oxygen atom. [a] our own experimental data.*

Carbon atom	***C1***	***C2***	***C3***	***C4***	***C5***	***C6***
$^{13}C\delta$ (Complex G)	98.7	85.7	79.9	84.1	70.3	63.1
$^{13}C\delta$ α-pyranose[a]	92.2	71.4	72.8	69.7	71.5	60.7
CIS value	**6.5**	**14.3**	**7.1**	**14.4**	**-1.2**	**2.4**
$^{13}C\delta$ β-pyranose[a]	96.0	74.2	76.0	69.7	75.8	60.8
CIS value	**2.7**	**11.5***	**3.9**	**14.4***	**-5.5**	**2.3**
$^{13}C\delta$ α-furanose[9]	97.6	76.7	76.3	78.7	70.1	64.1
CIS value	**1.1**	**9.0***	**3.6**	**5.4**	**0.2**	**-1.0**
$^{13}C\delta$ β-furanose[9]	103.2	81.2	75.6	81.6	70.5	64.3
CIS value	**-4.5**	**4.5**	**4.3**	**2.5**	**-0.2**	**-1.2**
$^{13}C\delta$ Hydrate form[8]	90.3	74.3	71.0	72.6	72.5	64.2
CIS value	**8.4***	**11.4***	**8.9***	**11.5***	**-2.2**	**-1.1**

Table S5. *Experimental ^{13}C NMR Chemical shifts (in ppm) of* ***complex H*** *and the corresponding experimental CIS value patterns of the assumed ligands. * Asterisk indicates a possible chelation site through an oxygen atom. [a] from theoretical calculations. [b] the chemical shift of the first carbon atoms is attributed by analogy with hydrated mannose.*

Carbon atom	***C1***	***C2***	***C3***	***C4***
$^{13}C\delta$ (Complex H)	93.5	92.6	80.2	71.3
α-furanose[a]	96.7	73.7	71.1	72.1
CIS value	**-3.2**	**18.9***	**9.1***	**-0.8**
β-furanose[a]	104.6	81.6	74.2	71.3
CIS value	**-11.1**	**11.0***	**6.0***	**0.0**
Hydrate form[8,b]	90.6	73.2	73.2	63.9
CIS value	**2.9***	**19.4***	**7.0***	**7.4***

Table S6. *Experimental ^{13}C NMR Chemical shifts (in ppm) of* ***complex I*** *and the corresponding experimental CIS value patterns of the assumed ligands. * Asterisk indicates a possible chelation site through an oxygen atom. [a] from theoretical calculations. [b] the chemical shift of the first carbon atoms is attributed by analogy with hydrated mannose.*

Carbon atom	***C1***	***C2***	***C3***	***C4***
$^{13}C\delta$ (Complex I)	94.3	93.2	80.6	71.8
α-furanose[a]	96.7	73.7	71.1	72.1
CIS value	**-2.4**	**19.5***	**9.5***	**0.6**
β-furanose[a]	104.6	81.6	74.2	71.3
CIS value	**-10.3**	**11.6***	**9.5***	**0.5**
Hydrate form[8,b]	90.6	73.2	73.2	63.9

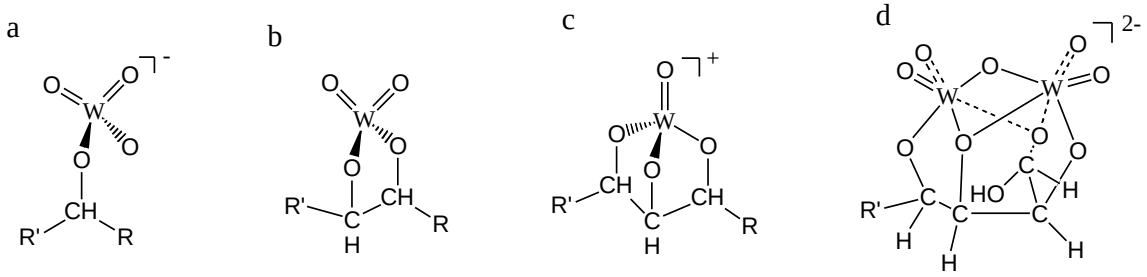

Figure S20. *Geometry of mononuclear (a) monodentate, (b) bidentate, (c) tridentate and dinuclear (d) tetradentate tungstate and molybdate complexes of sugars (glucose, mannose and erythrose) chosen as starting points for DFT calculations. All models feature W^{6+} and Mo^{6+} cores, hence the proposed charge state.*

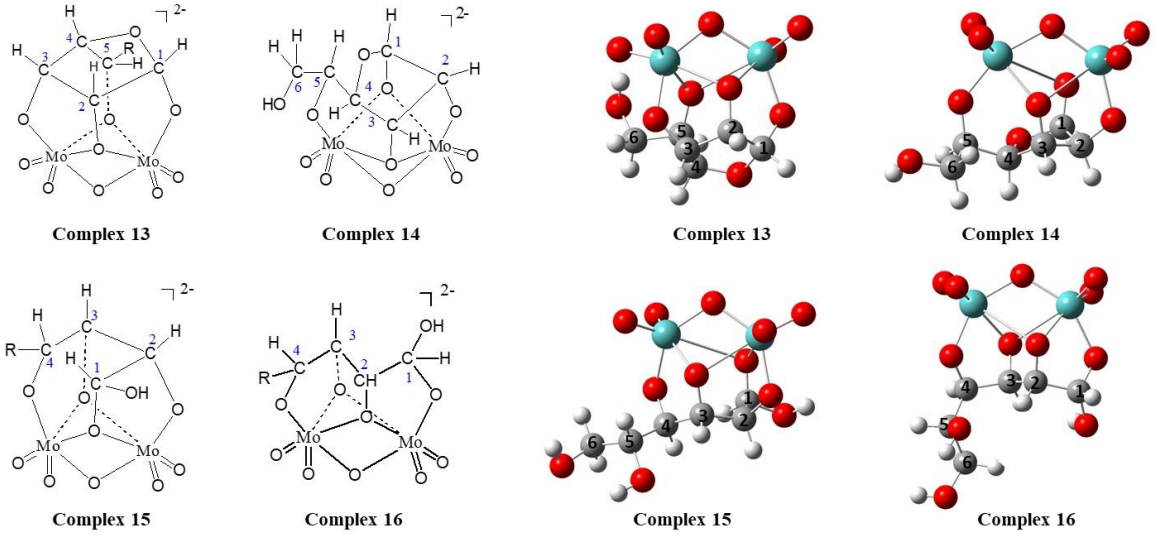

Figure S21. *Suggested complex models for complex E according to experimental NMR data. Complex models shown to the right represent the structure of each model optimized by DFT. C: gray, O: red, H: white and Mo: blue.*

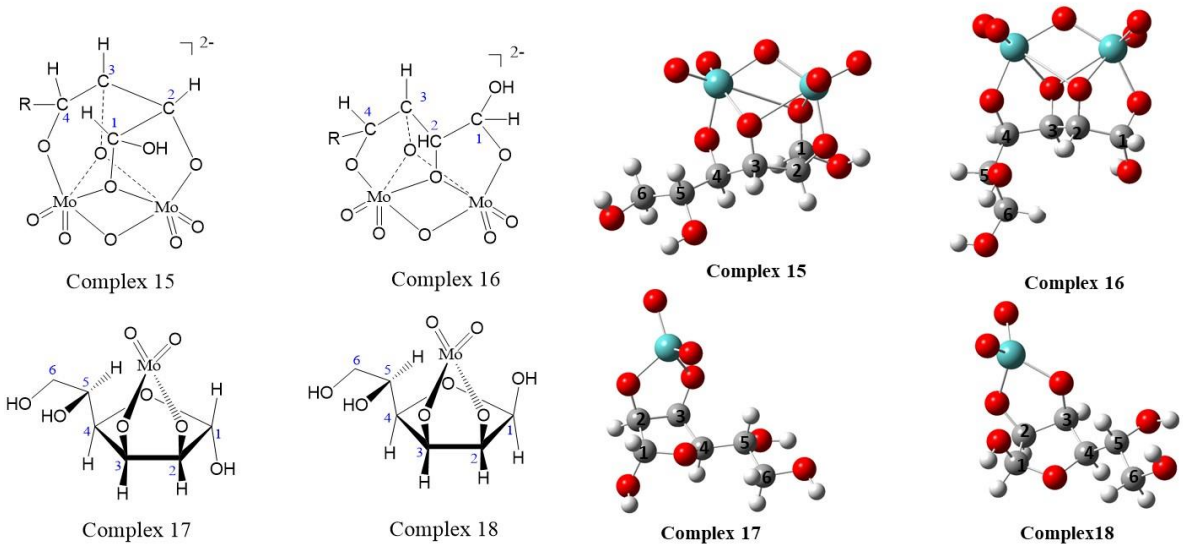

Figure S22. *Suggested complex models for complex F according to experimental NMR data. Complex models shown to the right represent the structure of each model optimized by DFT. C: gray, O: red, H: white and Mo: blue.*

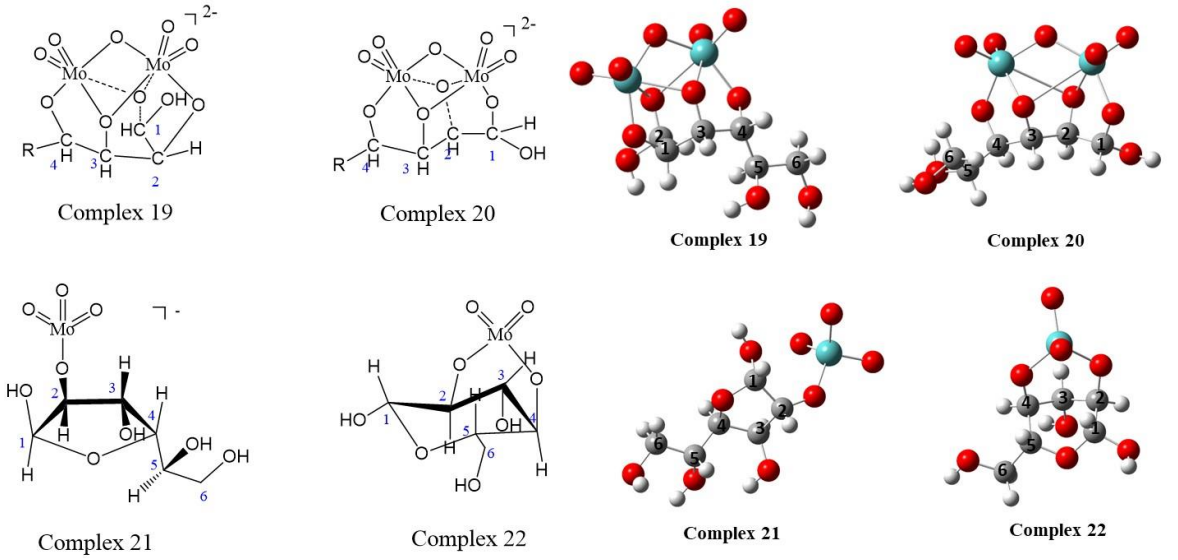

***Figure S23**. Suggested complex models for complex G according to experimental NMR data. Complex models shown to the right represent the structure of each model optimized by DFT. C: gray, O: red, H: white and Mo: blue.*

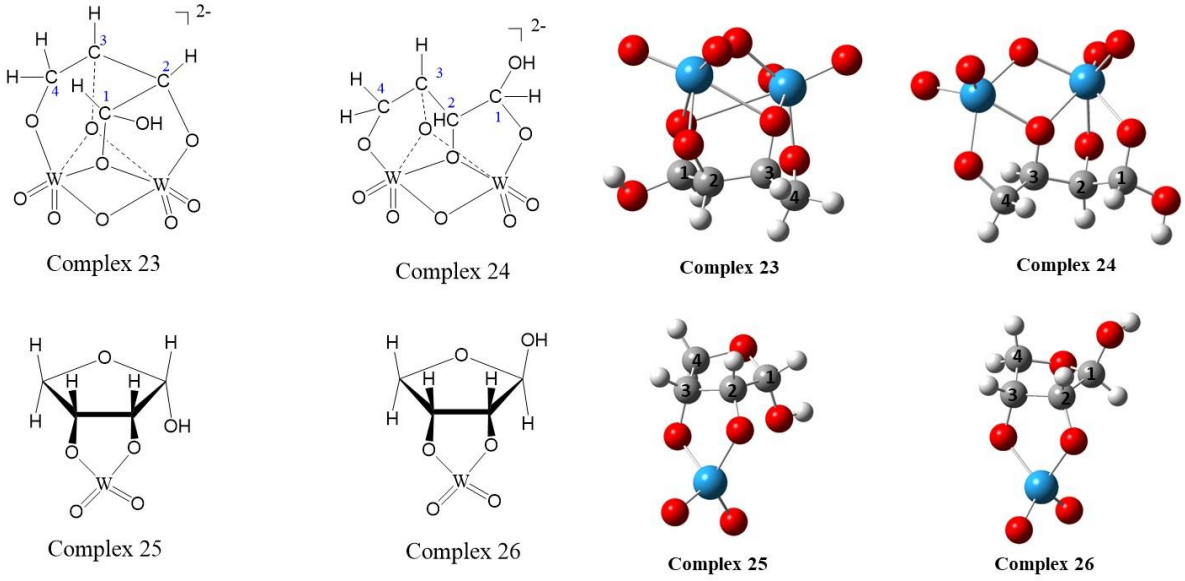

***Figure S24.** Suggested complex models for complex H according to experimental NMR data. Complex models shown to the right represent the structure of each model optimized by DFT. C: gray, O: red, H: white and Mo: blue.*

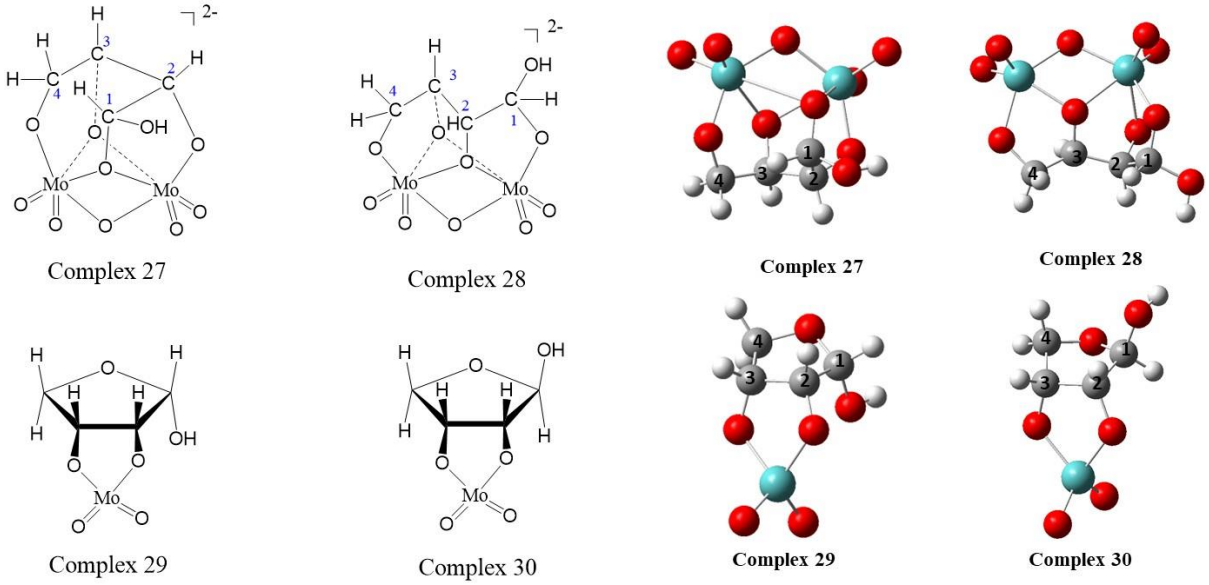

Figure S25. *Suggested complex models for complex I according to experimental NMR data. Complex models shown to the right represent the structure of each model optimized by DFT. C: gray, O: red, H: white and Mo: blue.*

Table S7. *Experimental ^{13}C NMR chemical shifts of complexes E and F in addition to the calculated ^{13}C NMR chemical shifts of the possible models of complexes suggested according to the experimental CIS values calculated and depicted in* ***Tables S2*** and ***S3.*** *The structures of the proposed complexes are illustrated in* ***Figures S13, S14.*** **Asterisk indicates a chelation site through the corresponding oxygen atom.* $\Delta\delta_{exp,th} = \delta_{exp} - \delta_{th}$.

Carbon atom	***C1***	***C2***	***C3***	***C4***	***C5***	***C6***
Complex E	***111.6***	***83.5***	***87.7***	***79.2***	***78.7***	***64.3***
Complex 13	*115.8**	*81.8**	*89.6**	*80.5*	*75.3**	*62.2*
$\Delta\delta_{exp,th}$	**-4.2**	**+1.7**	**-2.1**	**-1.3**	**+3.4**	**+2.1**
Complex 14	*107.4**	*92.2**	*74.2**	*77.0*	*83.8**	*65.7*
$\Delta\delta_{exp,th}$	**+4.2**	**-8.7**	**+13.3**	**+2.2**	**-5.1**	**-1.4**
Complex 15	*99.1**	*98.0**	*81.8**	*82.0**	*72.2*	*65.8*
$\Delta\delta_{exp,th}$	**+12.5**	**-14.5**	**+5.7**	**-2.8**	**+6.5**	**-1.5**
Complex 16	*103.6**	*84.0**	*75.5**	*87.8**	*76.9*	*65.9*
$\Delta\delta_{exp,th}$	**+8.0**	**-0.5**	**+12.0**	**-8.6**	**+1.8**	**-1.6**
Complex F	***94.5***	***93.4***	***81.0***	***80.5***	***71.1***	***63.4***
Complex 15	*99.1**	*98.0**	*81.8**	*82.0**	*72.2*	*65.8*
$\Delta\delta_{exp,th}$	**-4.6**	**-4.6**	**-0.8**	**-1.5**	**-1.1**	**-2.4**
Complex 16	*103.6**	*84.0**	*75.5**	*87.8**	*76.9*	*65.9*
$\Delta\delta_{exp,th}$	**-9.1**	**+9.4**	**+5.5**	**-7.3**	**-5.8**	**-2.5**
Complex 17	*105.7*	*112.4**	*109.3**	*83.0*	*68.4*	*65.8*
$\Delta\delta_{exp,th}$	**-11.2**	**-19.0**	**-28.3**	**-2.5**	**+2.7**	**-2.4**
Complex 18	*98.6*	*103.5**	*103.0**	*82.1*	*70.8*	*66.0*
$\Delta\delta_{exp,th}$	**-4.1**	**-10.1**	**-22.0**	**-1.6**	**+0.3**	**-2.6**

Table S8. *Experimental ^{13}C NMR chemical shifts of complex G in addition to the calculated ^{13}C NMR chemical shifts of the possible models of complexes suggested according to the experimental CIS values calculated and depicted in* ***Table S4.*** *The structures of the proposed complexes are illustrated in* ***Figures S15.*** **Asterisk indicates a chelation site through the corresponding oxygen atom.* $\Delta\delta_{exp,th} = \delta_{exp} - \delta_{th}$.

Carbon atom	***C1***	***C2***	***C3***	***C4***	***C5***	***C6***
Complex G	***98.7***	***85.7***	***79.9***	***84.1***	***70.3***	***63.1***
Complex 19	*98.2**	*98.9**	*80.9**	*84.1**	*74.3*	*64.5*
$\Delta\boldsymbol{\delta_{exp,th}}$	**+0.5**	**-13.2**	**-1.0**	**0.0**	**-4.0**	**-1.4**
Complex 20	*102.8**	*82.0**	*75.8**	*82.8**	*79.1*	*65.1*
$\Delta\boldsymbol{\delta_{exp,th}}$	**-4.1**	**+3.7**	**+4.1**	**+1.3**	**-8.8**	**-2.0**
Complex 21	*97.5*	*90.2**	*78.0*	*77.2*	*72.5*	*65.9*
$\Delta\boldsymbol{\delta_{exp,th}}$	**+1.2**	**-4.5**	**+1.9**	**+6.9**	**-2.2**	**-2.8**
Complex 22	*101.8*	*86.8**	*77.1*	*81.0**	*80.5*	*63.7*
$\Delta\boldsymbol{\delta_{exp,th}}$	**-3.1**	**-1.1**	**+2.8**	**+3.1**	**-10.2**	**-0.6**

Table S9. *Experimental ^{13}C NMR chemical shifts of complexes H and I in addition to the calculated ^{13}C NMR chemical shifts of the possible models of complexes suggested according to the experimental CIS values calculated and depicted in* ***Tables S5*** and ***S6.*** *The structures of the proposed complexes are illustrated in* ***Figures S16.*** **Asterisk indicates a chelation site through the corresponding oxygen atom.* $\Delta\delta_{exp,th} = \delta_{exp} - \delta_{th}$.

Carbon atom	***C1***	***C2***	***C3***	***C4***
Complex H	***93.5***	***92.6***	***80.2***	***71.3***
Complex 23	*97.9**	*94.5**	*79.0**	*68.4**
$\Delta\boldsymbol{\delta_{exp,th}}$	**-4.4**	**-1.9**	**+1.2**	**+2.9**
Complex 24	*97.6**	*77.9**	*88.0**	*63.4**
$\Delta\boldsymbol{\delta_{exp,th}}$	**-4.1**	**+14.7**	**-7.8**	**+7.9**
Complex 25	*97.5*	*94.0**	*96.2**	*72.5*
$\Delta\boldsymbol{\delta_{exp,th}}$	**-4.0**	**-1.4**	**-16.0**	**-1.2**
Complex 26	*105.8*	*106.1**	*100.4**	*73.1*
$\Delta\boldsymbol{\delta_{exp,th}}$	**-12.3**	**-13.5**	**-20.2**	**-1.8**
Complex I	***94.3***	***93.2***	***80.6***	***71.8***
Complex 27	*98.5**	*99.9**	*81.1**	*70.2**
$\Delta\boldsymbol{\delta_{exp,th}}$	**-4.2**	**-6.7**	**-0.5**	**+1.6**
Complex 28	*97.9**	*81.3**	*91.1**	*63.1**
$\Delta\boldsymbol{\delta_{exp,th}}$	**-3.6**	**+11.9**	**-10.5**	**+8.7**
Complex 29	*97.7*	*101.1**	*100.7**	*72.6*
$\Delta\boldsymbol{\delta_{exp,th}}$	**-3.4**	**-7.9**	**-20.1**	**-0.8**
Complex 30	*106.3*	*114.1**	*107.1**	*73.5*
$\Delta\boldsymbol{\delta_{exp,th}}$	**-12.0**	**-20.9**	**-26.5**	**-1.7**

Complex Assignment

Potential ligands were selected with respect to the deshielding of the carbon atoms bearing oxygen donor adducts by the Coordination Induced Shift (CIS) factor reported in Tables S2 to S6. This analysis has taken into consideration the geometry of each ligand since sugars occur naturally in 6 different cyclic and acyclic configurations. A minimum threshold for the downfield shift displayed at a coordinating carbon atom has been perceived to be of 5 ppm according to literature data.

- For the assignment of complex E (Table S2), by proposing α- and β- pyranose as ligands, four high coordination induced chemical shifts values at the first four carbon atoms of the two anomers were observed, indicating that four chelation sites exist through their deprotonated hydroxyl groups. However, these trans-orientated oxygen donors make the proposed chelation model inconceivable. The CIS patterns calculated by assuming α- and β-furanose as ligands, indicates that C1,2,3,5 are deshielded, thus O1,2,3,5 (numbered similarly as the carbon atom connected to O) should be the potential chelation sites. However, α- furanose features a trans-oriented oxygen atom at the C1 position compared to O2,3 site with respect to the ring plan, thus making such proposition only feasible for β-furanose in which HO1,2,3 are cis-oriented with each other with respect to the ring. Moreover, by supposing the acyclic hydrate mannose as a ligand, four high CIS values appear at the first four vicinal carbon atoms C1,2,3,4. The simulated structures are shown in Figure S21.
- As for complex F (Table S3), three high induced chemical shifts are displayed at the O2,3,4 site by proposing α- and β-mannopyranose as ligands. However, the hydroxyl group of the fourth carbon atom is trans-oriented to the O2,3 site with respect to the ring plan discarding their possibilities of being proper adducts for complex F. α- and β-furanose constitute proper candidates by displaying two high coordination induced shifts at their O2,3 site raising the possibility of the presence of a bidentate complex. By considering the hydrated mannose as a ligand, three downfield shifts higher than 5 ppm were detected at O2,3,4 possible coordination site. However, according to the DFT data that will be further discussed, hydrated mannose probably chelates the metal ion through four deprotonated oxygen atoms (O1,2,3,4 site) displaying only a little shift at the first carbon atom. The simulated structures are shown in Figure S22.
- Regarding complex G (Table S4), four high induced chemical shifts were calculated at the O1,2,3,4 site of the α-pyranose tautomer featuring trans-oriented O3 and O1,2,4 (Figure S23) donor adducts with respect to the ring which makes the proposed coordination inconvincible. With β-pyranose, two high induced chemical shifts are observed at the O2,4 site, indicating the potential presence of a bidentate complex. The calculations with α-furanose shows a single high CIS value at the second carbon position bearing an oxygen donor (at the fourth carbon atom no

oxygen donor exists) indicating the possibility of the presence of a monodentate complex through the O2 site. Finally, by supposing the acyclic hydrate glucose as a ligand, four high CIS values appear at the first four vicinal carbon atoms C1,2,3,4 proposing O1,2,3,4 adducts as a potential chelation site.

- Tungstate-erythrose complex H and molybdate-erythrose complex I (Tables S5 and S6) show similar behaviours for the calculation of CIS values with respect to erythrose tautomers (Figure S24). With α- and β- furanose proposed as ligands, two high CIS values are observed at the O2,3 site indicating that a potential bidentate complex could exist with both metals and furanose forms. Moreover, the CIS value calculated by considering hydrated erythrose as a potential ligand, we observe a significant downfield shift at the C1,2,3,4 carbon atoms (further confirmed by DFT for C1) indicating that a chelation possible through O1,2,3,3 site.

It should be mentioned that the same analysis was done for complexes A, B, C and D for tungstate-mannose complexes in our previous study (Inorg. Chem. 2023, 62, 7545−7556). Moreover, acyclic aldehyde forms of the sugars were discarded since no signal was acquired at around 200 ppm which is a fingerprint of the existence of a carbonyl group.

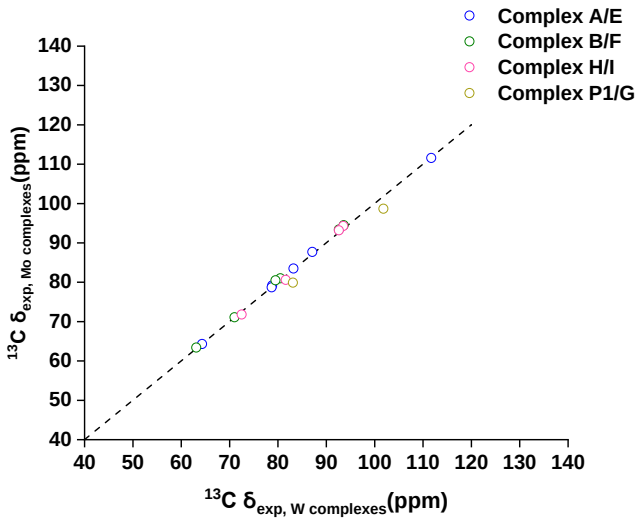

Figure S26. *Correlation curve of ^{13}C NMR chemical shifts of the experimentally observed isostructural tungstate and molybdate complexes.*

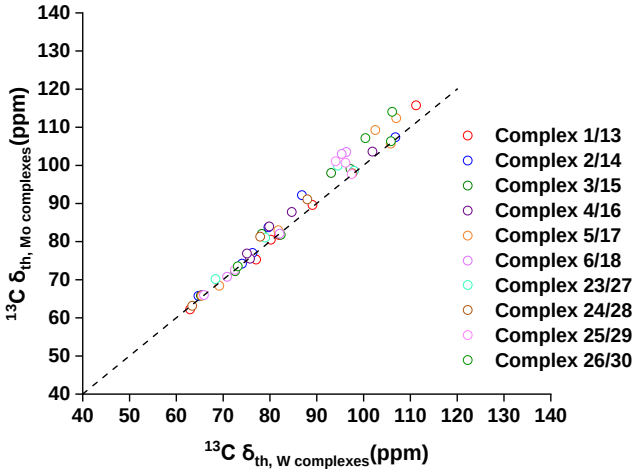

Figure S27*. Correlation curve of ^{13}C NMR chemical shifts of all the proposed models for tungstate and molybdate complexes of sugars (complex models are shown in the supporting Information ,* ***Figures S13****,* ***S14****,* ***S15*** *and* ***S16.*** *Each complex model was optimized and calculated with Mo and W).*

Energy data

We evaluated the energetics of the formation of each complex according to the general ***Equation S1*** (M = Mo or W). All elements are considered as solvated in water. For all components but H_2O and H^+, the solvation energy was estimated by the SMD model. For water and H^+, we used the computed gas-phase data and added experimental solvation energies as the one computed did not yield satisfactory results *wrt* the experimental data, especially for H^+.[1] The values employed were taken from the literature[10–12] and are listed in ***Table S1***. All values are calculated at 298.15 K from the 0 K energy and vibrational analysis as implemented in Gaussian09 and given with all components in their standard state in aqueous solution at 1 M.

$$C_6H_{12}O_6 + xMO_4^{2-} + yH^+ = M_xO_z\left(C_6H_{12+y-8x-2z}O_6\right)^{y-2x} + (4x-z)H_2O \qquad \textbf{Equation S1}$$

Table S10. *Structural detail and energetic data for the formation of the complexes reported in the manuscript. "Denticity" indicates the number of oxygen atoms of the sugar involved in the complex. "Exp." refers to the assignment to the experimentally observed species. Energetic data are calculated at 298.15 K from the 0 K energy and vibrational analysis as implemented in Gaussian09. G and H expressed in kJ mol^{-1}, S in J K^{-1} mol^{-1}. Complexes from number 1 to 12 are the proposed models for tungsten-mannose complex structures already reported in the supplementary information of our previous article.* [1]

Complex	Metal/Sugar	Tautomer	Nuclearity	Denticity	Coordination mode	$\Delta_rH°$	$\Delta_rS°$	$\Delta_rG°$	Exp.
1	W/Mannose	β-furanose	dinuclear	tetradentate	O1,2,3,5 ; Bridging O2,5	-36	**-8**	-34	A
2	W/Mannose	β-furanose	dinuclear	tetradentate	O1,2,3,5 ; Bridging O1,3	-54	**7**	-56	
3	W/Mannose	acyclic hydrate	dinuclear	tetradentate	O1,2,3,4 ; Bridging O1,3	-36	**-69**	-15	B
4	W/Mannose	acyclic hydrate	dinuclear	tetradentate	O1,2,3,4 ; Bridging O2,3	-45	**-69**	-24	
5	W/Mannose	α-furanose	mononuclear	bidentate	O2,3	-28	**118**	-63	
6	W/Mannose	β-furanose	mononuclear	bidentate	O2,3	-27	**126**	-64	
7	W/Mannose	α-furanose	dinuclear	tetradentate	O2,3,5,6 ; Bridging O3,5	-45	**11**	-48	C
8	W/Mannose	α-furanose	dinuclear	tetradentate	O2,3,5,6 ; Bridging O2,5	-54	**1**	-55	
9	W/Mannose	β-furanose	dinuclear	pentadentate	O1,2,3,5,6 ; Bridging O3	58	**-35**	69	
10	W/Mannose	β-furanose	dinuclear	pentadentate	O1,2,3,5,6 ; Bridging O1	83	-43	96	
11	W/Mannose	α-furanose	mononuclear	monodentate	O2	-56	**-4**	-54	D
12	W/Mannose	β-furanose	mononuclear	tridentate	O1,2,3	98	**252**	23	
13	Mo/Mannose	β-furanose	dinuclear	tetradentate	O1,2,3,5 ; Bridging O2,5	-31	**-42**	-19	E
14	Mo/Mannose	β-furanose	dinuclear	tetradentate	O1,2,3,5 ; Bridging O1,3	-38	**-27**	-37	
15	Mo/Mannose	acyclic hydrate	dinuclear	tetradentate	O1,2,3,4 ; Bridging O1,3	-34	**-122**	3	F
16	Mo/Mannose	acyclic hydrate	dinuclear	tetradentate	O1,2,3,4 ; Bridging O2,3	-22	**-117**	13	
17	Mo/Mannose	α-furanose	mononuclear	bidentate	O2,3	-34	**112**	-68	
18	Mo/Mannose	β-furanose	mononuclear	bidentate	O2,3	-33	**99**	-62	
19	Mo/Glucose	acyclic hydrate	dinuclear	tetradentate	O1,2,3,4 ; Bridging O1,3	-26	**-134**	14	
20	Mo/Glucose	acyclic hydrate	dinuclear	tetradentate	O1,2,3,4 ; Bridging O2,3	-32	**-130**	7	G
21	Mo/Glucose	α-furanose	mononuclear	monodentate	O2	-56	-44	**-42**	
22	Mo/Glucose	β-pyranose	mononuclear	bidentate	O2,4	-26	+85	**-51**	
23	W/Erythrose	acyclic hydrate	dinuclear	tetradentate	O1,2,3,4 ; Bridging O1,3	-51	**-86**	-26	H
24	W/Erythrose	acyclic hydrate	dinuclear	tetradentate	O1,2,3,4 ; Bridging O2,3	30	-90	**57**	
25	W/Erythrose	α-furanose	mononuclear	bidentate	O2,3	-31	+121	**-67**	
26	W/Erythrose	β-furanose	mononuclear	bidentate	O2,3	-42	+101	**-72**	
27	Mo/Erythrose	acyclic hydrate	dinuclear	tetradentate	O1,2,3,4 ; Bridging O1,3	-35	**-141**	7	I
28	Mo/Erythrose	acyclic hydrate	dinuclear	tetradentate	O1,2,3,3 ; Bridging O2	43	+119	**7**	
29	Mo/Erythrose	α-furanose	mononuclear	bidentate	O2,3	-43	+85	**-68**	

30	Mo/Erythrose	β-furanose	mononuclear	bidentate	O2,3	-48	+69	**-68**

References

(1) El Mohammad, S.; Proux, O.; Aguilar, A.; Hazemann, J. L.; Legens, C.; Chizallet, C.; Larmier, K. Elucidation of Metal-Sugar Complexes: When Tungstate Combines with D-Mannose. *Inorganic Chemistry* **2023**, *62*, 7545–7556.

(2) Puigdomenech, I. *Medusa*; KTH. https://www.kth.se/che/medusa (accessed 2023-01-27).

(3) Chapelle, S.; Verchère, J.-F. Tungstate complexes of aldoses and ketoses of the lyxo series. Multinuclear NMR evidence for chelation by one or two oxygen atoms borne by the side chain of the furanose ring. *Carbohydrate research* **1995**, *277*, 39–50.

(4) Sauvage, J.-P.; Chapelle, S.; Dona, A.-M.; Verchère, J.-F. Acyclic molybdate complexes of aldoses in the arabino and xylo series and their application to the determination of the proportion of acyclic forms in aqueous solution. *Carbohydrate research* **1993**, *243*, 293–305.

(5) Bilik, V.; Matulova, M. Reactions of saccharides catalyzed by molybdate ions XLII. Epimerization and the molybdate complexes of aldoses. *Chemical Papers* **1990**, *44*, 257–265.

(6) Matulova, M.; Verchère, J.-F.; Chapelle, S. Furanose vs. acyclic forms of carbohydrate ligands. A multinuclear NMR spectroscopy of the molybdate and tungstate complexes of D-glycero-L-manno-heptose. *Carbohydrate research* **1996**, *287*, 37–48.

(7) Verchère, J.-F.; Chapelle, S. Stability constants and structures of homologous dinuclear molybdate and tungstate complexes of aldoses by potentiometry and 13C and 95Mo NMR. *Polyhedron* **1989**, *8* (3), 333–340.

(8) Zhu, Y.; Zajicek, J.; Serianni, A. S. Acyclic forms of [1-13C]aldohexoses in aqueous solution: quantitation by 13C NMR and deuterium isotope effects on tautomeric equilibria. *The Journal of Organic Chemistry* **2001**, *66* (19), 6244–6251. DOI: 10.1021/jo010541m.

(9) Alexandersson, E.; Nestor, G. Complete 1H and 13C NMR spectral assignment of D-glucofuranose. *Carbohydrate research* **2022**, *511*, 108477. DOI: 10.1016/j.carres.2021.108477. Published Online: Nov. 9, 2021.

(10) Coe, J. V. Connecting cluster ions and bulk aqueous solvation. A new determination of bulk single ion solvation enthalpies. *Chemical Physics Letters* **1994**, *229*, 161–168.

(11) Mejias, J. A.; Lago, S. Calculation of the absolute hydration enthalpy and free energy of H+ and OH-. *The Journal of Chemical Physics* **2000**, *113*, 7306.

(12) Palascak, M. W.; Shields, G. C. Accurate Experimental Values for the Free Energies of Hydration of H+ , OH- , and H3O+. *J. Phys. Chem. A* **2004**, *108* (16), 3692–3694. DOI: 10.1021/jp049914o.